



# Influence of $P_2O_5$ addition on glass structure and luminescent properties of $Eu^{3+}$ ions in $SiO_2$ – $CaO$ particles of bioactive glass

Beata Borak<sup>1,a</sup>, Jolanta Szczurek<sup>1</sup>, Katarzyna Halubek-Gluchowska<sup>2</sup>, Anna Lukowiak<sup>2,b</sup>

<sup>1</sup> Department of Mechanics, Materials and Biomedical Engineering, Wrocław University of Science and Technology, Smoluchowskiego 25, 50-370 Wrocław, Poland

<sup>2</sup> Institute of Low Temperature and Structure Research, PAS, ul. Okolna 2, 50-422 Wrocław, Poland

Received: 7 November 2023 / Accepted: 26 December 2023

© The Author(s), under exclusive licence to Società Italiana di Fisica and Springer-Verlag GmbH Germany, part of Springer Nature 2024

**Abstract** Phosphorous compounds are essential for living organisms, specifically as building blocks for hard tissues such as bones. Therefore, it is an important (although not necessary) component of bioactive glass used in regenerative medicine. Hereby, the influence of  $PO_4^{3-}$  on the properties of silica–calcium glass was studied. Europium(III) ions, as a luminescent probe, have been incorporated into bioactive glass hosts of both binary ( $SiO_2$ – $CaO$ ) and ternary ( $SiO_2$ – $CaO$ – $P_2O_5$ ) systems obtained via sol–gel technique. The fabricated glasses consisted of spherical particles with an average diameter close to 100 nm. The energy dispersive X-ray analysis confirmed the presence of silicon, calcium, phosphorous, and europium ions, although with different ratios than assumed during the synthesis process. The lower amount of calcium oxide was detected mainly in the silica–calcium composition (16 wt.% instead of 35 wt.%). The presence of phosphate groups in the glass allowed for the maintenance of a higher CaO concentration (23 wt.%), but partial crystallization of the material occurred, which was not observed in the binary system. Investigation of the photoluminescent properties showed that  $Eu^{3+}$  emission had higher intensity and longer decay times when samples were annealed at higher temperatures (the tested temperature range was 600–800 °C), indicating reduced hydroxyl quenching. The addition of phosphate groups resulted in shorter luminescence lifetimes in comparison to the  $SiO_2$ – $CaO$  samples due to the modified environment of europium ions caused by partial crystallization.

## 1 Introduction

Bioactivity is a unique feature of various types of glasses (silicate-, borate-, and phosphate-based systems) [1] that is not obvious to many researchers even those working with glasses. These materials show osteoinductive behaviour and have the ability to form an interfacial bond with soft and hard tissues when incorporated into the body or exposed to a biological fluid. In their composition, calcium and phosphorous are often present — the same elements that are the main components of biological apatites. As such, these ions play an important role in bone formation and resorption. Calcium is known to affect osteoblastic cells and is required for osteoblast proliferation, differentiation, and mineralization [2]. Phosphorous in inorganic phosphate is claimed to stimulate the expression of matrix Gla protein, which is a key regulator for bone formation in osteoblastic cells [2]. Among other ions, silicon Si is known to increase bone mineral density and improve bone strength. Taking part in metabolic processes, Si leads to the formation and calcification of bone tissue and also induces the precipitation of hydroxyapatite [2, 3]. Formed in physiological conditions, orthosilicic acid ( $Si(OH)_4$ ) is claimed to stimulate collagen type I formation in human osteoblast cells and osteoblastic differentiation [2–4].

Binary  $SiO_2$ – $CaO$ , ternary  $SiO_2$ – $CaO$ – $P_2O_5$ , quaternary  $SiO_2$ – $CaO$ – $P_2O_5$ – $Na_2O$  or  $SiO_2$ – $CaO$ – $P_2O_5$ – $MO$  ( $M = \text{metal}$ ) [5, 6], as well as more complex systems like  $SiO_2$ – $CaO$ – $CaF_2$ – $Na_2O$ – $K_2O$ – $P_2O_5$ – $MgO$  or  $SiO_2$ – $TiO_2$ – $B_2O_3$ – $P_2O_5$ – $CaO$ – $MgO$ – $K_2O$ – $Na_2O$  [7] are considered as bioactive. Initially, it was assumed that  $P_2O_5$  was required for glass to obtain bioactivity. Now, it is known that the presence of phosphate in the system is not necessary. The phosphate ions needed for the hydroxyapatite layer formation can be adsorbed from the body fluid or from the assay solution in the in vitro tests, for example, from simulated body fluid (SBF) [5, 8–10]. Due to this process, glasses in the binary system ( $SiO_2$ – $CaO$ ) also show bioactivity [5, 11] although, it is higher in the ternary systems with phosphorous oxide [12]. During glass degradation, both  $Ca^{2+}$  and  $PO_4^{3-}$  ions diffused into the surrounding solution cause its supersaturation which favors the formation of hydroxyapatite [12]. For this reason, phosphate is considered a significant component in bioactivity and apatite formation. To further improve the glass reactivity in the body fluids, different additives are

<sup>a</sup> e-mail: [Beata.Borak@pwr.edu.pl](mailto:Beata.Borak@pwr.edu.pl) (corresponding author)

<sup>b</sup> e-mail: [A.Lukowiak@intibs.pl](mailto:A.Lukowiak@intibs.pl) (corresponding author)

introduced into the glass structure, especially trace elements found in the human body: Ce, Ga, Zn, Cu, Mg, Sr, Co, and others [1, 2, 13–15]. Ag and Zn have been investigated as well to develop antibacterial materials [16].

The bioactivity of silica-based glasses comes from cation exchange, in which ions (calcium and  $\text{PO}_4^{3-}$ ) are replaced by protons from the body fluid [5, 9, 17]. As a result of this exchange, a silicon-rich layer is created on the glass surface, which is a base for hydroxyapatite, HA (or carbonated hydroxyapatite, HCA), formation. This layer is responsible for the strong bonding between bioactive glasses and human bones [2].

Bioactive glasses can be obtained by melting the proper oxides or carbonates in adequate proportions at a temperature above 1300 °C or at a lower temperature when the sol–gel method is applied [18]. In comparison to the conventional bioactive glasses obtained by the melt-quenching technique, the materials obtained by the sol–gel method often demonstrate higher bioactivity [19]. In general, the sol–gel process arrives at the formation of a mesoporous structure with a high surface area and surface chemistry rich in silanol groups that increases the degradation rate and promotes the formation of the hydroxy carbonate apatite layer. Silanol groups are involved in the nucleation of the HCA layer [19] and mesoporous structure accelerates the ion exchange rate between the material and the surrounding medium.

Another advantage of the sol–gel method is the possibility of glass functionalization or doping including optical activation with rare-earths (REs). The RE ions with their photoluminescent properties are attractive, for example, as optical probes [20]. Among activators, europium ( $\text{Eu}^{3+}$ ) ions are found to be particularly interesting. In  $\text{Eu}^{3+}$  ions the levels: ground  $^7\text{F}_0$  and the first excited  $^5\text{D}_0$  are non-degenerated ( $J = 0$ ) under any symmetry. It means that information connected with the local environment around  $\text{Eu}^{3+}$  ions is dependent only on the splitting of  $^5\text{D}_0 \rightarrow ^7\text{F}_J$  ( $J = 0-4$ ) transitions. The interaction between the europium ion and its surroundings induces changes in luminescence parameters such as intensity, position of the excitation and emission wavelengths, quantum efficiency, and luminescence decay time. All these variables cause that  $\text{Eu}^{3+}$  ions could be used to investigate the local environment around the lanthanide ions in different matrices [21, 22] including bioactive glasses. Research on these materials performed so far included studies on  $\text{Eu}^{3+}$ -doped bulk phosphate glasses ( $\text{P}_2\text{O}_5\text{--K}_2\text{O--MgO--Na}_2\text{O--CaO}$ ) obtained by melt-quenching [23], glass–ceramic scaffolds ( $\text{CaO--SiO}_2\text{--P}_2\text{O}_5\text{--MgO--CaF}_2$ ) [24], mesoporous glasses obtained by modified sol–gel technique [25, 26], or mesoporous nanofibers fabricated by electrospinning [27]. Among powders, 45S5 Bioglass® [28] and sol–gel-derived nanoparticles ( $\text{SiO}_2\text{--CaO}$  [29],  $\text{SiO}_2\text{--CaO--P}_2\text{O}_5$  [30],  $\text{SiO}_2\text{--Na}_2\text{O--K}_2\text{O--MgO--CaO--P}_2\text{O}_5$  [31, 32]) were investigated. The optical properties were used to follow not only the crystallization processes but also to track the delivery and release of drugs, cell labeling, or even to show glass potential for use in radiation dosimetry [25, 27, 29, 33]. However, there were no reports comparing the optical properties of europium-activated nanoparticles of binary and ternary glasses fabricated by the sol–gel method.

In the presented research, the modified Stöber method was used to obtain spherical nanoparticles of  $\text{Eu}^{3+}$ -doped  $\text{SiO}_2\text{--CaO}$  and  $\text{SiO}_2\text{--CaO--P}_2\text{O}_5$  glasses. Their morphology, composition, structure, and optical properties were described looking mainly at the influence of phosphate groups introduced into the network. The europium ions were used to monitor changes in the glass host environment caused by sample composition and annealing temperature.

## 2 Experimental

### 2.1 Synthesis

The bioactive glass samples in the binary system were prepared using the sol–gel synthesis route through a modified Stöber method performed in a two-step (acid-alkaline) process. The details of the  $\text{SiO}_2\text{--CaO}$  synthesis were reported previously [34, 35]. The same procedure with the necessary adaptations was followed to obtain a glass of the ternary system  $\text{SiO}_2\text{--CaO--P}_2\text{O}_5$ . In the latter case, phosphoric acid (85%) was used both to catalyze tetraethyl orthosilicate (TEOS, 99.9%) hydrolysis and as the  $\text{PO}_4^{3-}$  precursor. Briefly, TEOS was mixed with  $\text{Eu}(\text{NO}_3)_3$ , water, ethanol, and  $\text{H}_3\text{PO}_4$  (nitric acid was used in the case of binary glass) Then, the sol was slowly poured into basic water–ethanol solution under stirring. A few minutes later, calcium ions were added to the reaction mixture. Calcium nitrate tetrahydrate (>99%) and ammonium hydroxide (25%) were used as the Ca precursor and the base catalyst leading to particle condensation, respectively. The white gel particles obtained after the reaction were separated by centrifugation and washed with ethanol and water. The samples were dried at 80 °C for 24 h and afterward annealed for 2 h at the temperature of 600, 700, or 800 °C in the air. For the syntheses, the amount of substrates was calculated to obtain glass with the composition of  $64.4\text{SiO}_2:35\text{CaO}:0.6\text{Eu}_2\text{O}_3$  or  $59.6\text{SiO}_2:35\text{CaO}:5\text{P}_2\text{O}_5:0.4\text{Eu}_2\text{O}_3$  (wt.%), respectively (exact values are given in Table 1).

### 2.2 Morphological, structural, and composition analysis

The morphology and composition of the obtained samples were analyzed by scanning electron microscopy (FESEM FEI Nova NanoSEM) equipped with an energy dispersive X-ray (EDS) detector (EDAX Genesis). For the measurements, the samples were put on a carbon tape and covered with a carbon layer. The size distribution of the particles was estimated using SEM images and the ImageJ program. The composition analysis was carried out using EDS and an inductively coupled plasma optical emission spectrometer (ICP-OES, Thermo Scientific iCAP 7000). The amorphous or partially crystallized structure of the samples was analyzed by X-ray diffraction measurements (X'Pert PRO PANalytical, Cu  $\text{K}\alpha$  radiation 1.5406 Å).

**Table 1** Comparison between assumed composition of samples and EDS and ICP-OES quantification (wt.%). Data for sample annealed at 700 °C

	Assumed composition	EDS analysis	ICP-OES
	Eu <sup>3+</sup> :SiO <sub>2</sub> -CaO		
SiO <sub>2</sub>	64.39	86.5 ± 0.2	82.0 ± 4.0
CaO	35.02	11.7 ± 0.1	16.3 ± 2.0
Eu <sub>2</sub> O <sub>3</sub>	0.59	1.77 ± 0.09	1.7 ± 0.1
	Eu <sup>3+</sup> :SiO <sub>2</sub> -CaO-P <sub>2</sub> O <sub>5</sub>		
SiO <sub>2</sub>	59.67	68.9 ± 0.5	69.4 ± 4.0
CaO	34.70	19.8 ± 0.3	22.8 ± 2.0
P <sub>2</sub> O <sub>5</sub>	5.26	10.1 ± 0.4	6.3 ± 0.2
Eu <sub>2</sub> O <sub>3</sub>	0.38	1.26 ± 0.03	1.5 ± 0.1

### 2.3 Spectroscopic analysis

A microRaman apparatus (inVia™ Renishaw) with an 830 nm laser diode was used to collect Raman spectra. The photoluminescence and photoluminescence excitation spectra as well as the luminescence lifetimes were measured with a fluorescence spectrometer (FLS980 Edinburgh Instruments) equipped with a 450W xenon lamp and 150W pulse lamp. The measured spectra were corrected with respect to the detector sensitivity and lamp characteristics. The measurements were performed at room temperature. The photoluminescence excitation spectra were normalized to the peak of the most intense band. The experimental decays of photoluminescence were fitted with first- (binary system) or second-order (ternary system) exponential decay functions with the formulas:  $f(t) = A \cdot \exp(-t/\tau) + y_0$  and  $f(t) = A_1 \cdot \exp(-t/\tau_1) + A_2 \cdot \exp(-t/\tau_2) + y_0$ , respectively. In the latter case, the effective lifetime constant ( $\tau'$ ) was calculated as  $\tau' = (A_1 \cdot \tau_1^2 + A_2 \cdot \tau_2^2) / (A_1 \cdot \tau_1 + A_2 \cdot \tau_2)$  [36]. In the equations,  $\tau_1$  and  $\tau_2$  are rapid and slow decay times, respectively.

## 3 Results and discussion

### 3.1 Morphology

The proper procedure in the sol-gel synthesis method allows the fabrication of spherical silica-calcia particles. Using such a procedure, both binary SiO<sub>2</sub>-CaO and ternary SiO<sub>2</sub>-CaO-P<sub>2</sub>O<sub>5</sub> glass systems doped with europium(III) ions were prepared. Two steps, acid-base hydrolysis process was conducted to obtain powders which consisted of spherical particles with an average diameter of around 100 nm and a size distribution between 40 and 200 nm (Fig. 1). Synthesis with phosphoric acid, added to the reaction mixture instead of commonly used nitric acid (like in the case of SiO<sub>2</sub>-CaO), allowed not only to catalyze the hydrolysis reaction of TEOS but also to modify the composition and introduce phosphate groups. At the same time, the shape of the particles was not affected, although a slightly higher amount of bigger particles (100–160 nm) was observed (Fig. 1b). A base catalyst in the second step of the synthesis is needed to promote the precipitation of the particulate gel and the reduction of the gelation time. It is also claimed that ammonium hydroxide used as a catalyst to control the sol-gel condensation reaction, causes the formation of round-shaped particles which do not agglomerate [8]. Subsequent annealing of the powders led to the incorporation of calcium and phosphorous in the silica network. SEM images revealed that after heat treatment in the selected temperature range (600–800 °C), the particles did not undergo co-sintering.

### 3.2 Composition

The performed analysis quantified the ratios of oxides in the binary and ternary compositions. Table 1 shows the comparison between the initial (at the synthesis stage) and the final (EDS and ICP-OES analysis) amount of oxides in weight percentage (wt.%) for the samples annealed at 700 °C. The EDS and ICP-OES analyses indicated the presence of all introduced atoms (Si, Ca, P, and Eu), but the measured values showed deviations from the initial formulations. It was evident that the powders of both systems contained a lower amount of CaO than was initially assumed, and it was between 12 wt.% and 23 wt.%, depending on the sample and measurement technique (Table 1). Simultaneously, with lower calcium content, the silicon and phosphorous amount increased. The content of Eu<sub>2</sub>O<sub>3</sub> is also above the original set value. Based on the more accurate ICP-OES analysis, the amount of Eu<sup>3+</sup> ions should be equal to 0.59 mol% and 0.52 mol% in the binary and ternary glass, respectively.

The reason why CaO is lower than assumed is related to the used procedure, mainly because of the washing process carried out immediately after synthesis. Free calcium ions were partially removed during the washing step used to remove the byproducts or ammonia. Calcium precursor is added as the last ingredient during the synthesis, and therefore, Ca<sup>2+</sup> ions are present mainly on the surface of the particles and can be easily removed.

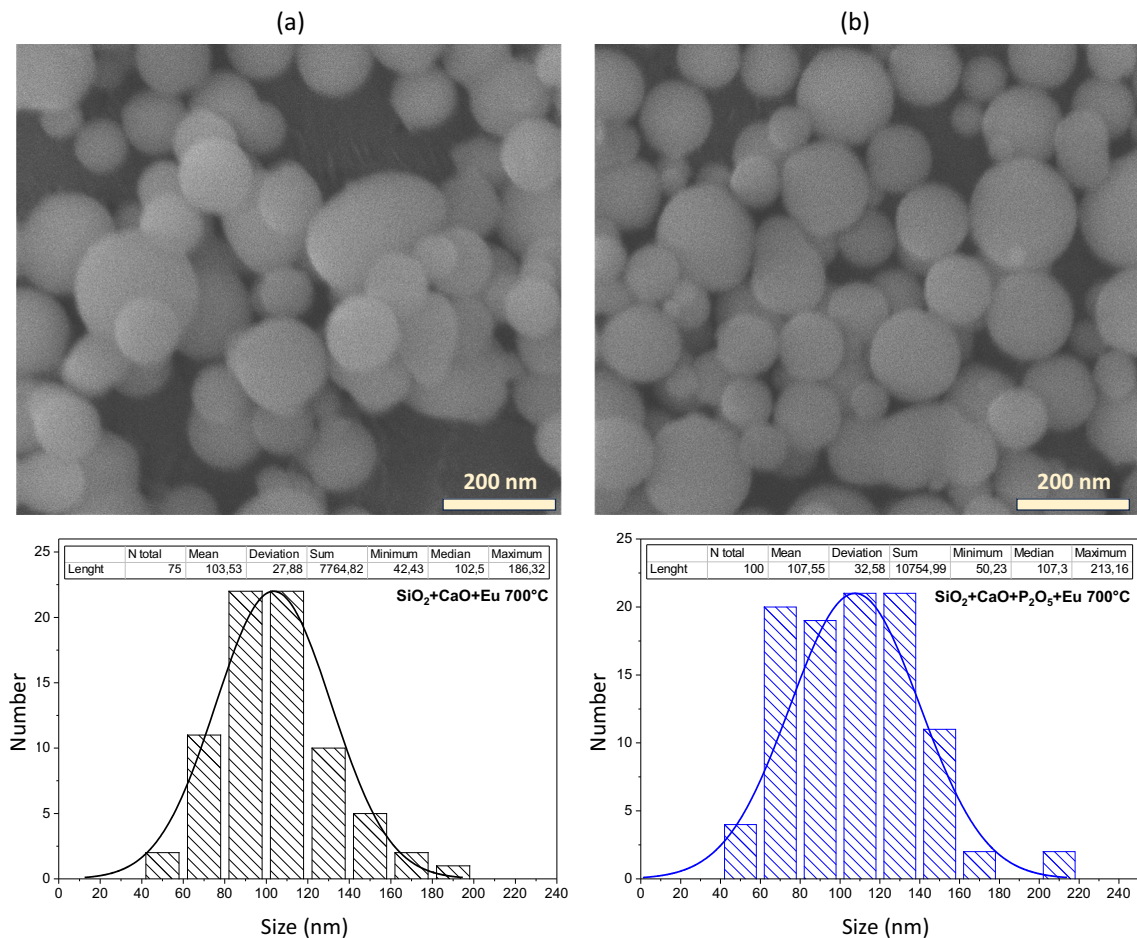


**Fig. 1** SEM images of  $\text{Eu}^{3+}:\text{SiO}_2\text{--CaO}$  (a) and  $\text{Eu}^{3+}:\text{SiO}_2\text{--CaO--P}_2\text{O}_5$  (b) particles annealed at 700 °C with particle size distribution

At this point, it must be noted that in the case of phosphate samples, not fully amorphous systems were obtained, and not only oxides but other phases, such as calcium phosphates, were present (as discussed in the next chapter). The formation of additive calcium compounds with phosphate groups might lead to higher  $\text{Ca}^{2+}$  content in the ternary system.

### 3.3 Structure

The diffractograms of the obtained powders reflected the amorphous nature of this material showing broad reflection centered around  $23^\circ$  (Fig. 2). In the case of samples containing  $\text{P}_2\text{O}_5$ , partial crystallization was seen, which increased slightly with the annealing temperature. As was previously indicated, crystallization in the binary  $\text{Eu}^{3+}:\text{SiO}_2\text{--CaO}$  glass occurred above 800 °C [35], showing first quartz and then pseudowollastonite and cristobalite phases. Thus, a higher annealing temperature was not used for the investigated samples. Here, it was evident that in the ternary system, the presence of  $\text{PO}_4^{3-}$  led to the crystallization of phosphates such as tricalcium bis(phosphate(V))  $\text{Ca}_3(\text{PO}_4)_2$  (ICSD #200,202) and decacalcium hexakis(phosphate(V)) oxide  $\text{Ca}_{10}(\text{PO}_4)_6\text{O}$  (ICSD #87,727). The gamma dicalcium silicate,  $\gamma\text{-Ca}_2\text{SiO}_4$ , (ICSD #417,503) phase was also marked in the diffractograms.

It was previously observed that the crystallinity of bioactive glasses increased with higher phosphate content [37]. It should be mentioned here that crystallization is not a demanded process for bioactive glass fabrication. It decreases the dissolution rate of glass components, restricts ion mobility, and has a detrimental effect on bioactivity because prevents the hydroxyapatite layer from being created. In some cases, it may turn bioglass into a bioinert material [37].

Thermal treatment of the glasses is needed for three reasons: to incorporate calcium into the glass network (temperature above 450 °C), to remove organic residuals (>500 °C), and to remove nitrate byproducts (>600 °C) [8]. Higher temperatures of annealing (>1000 °C) cause melting and co-sintering of the particles in large aggregates as well as crystallization. In the processing of bioactive glasses, it is important to have the particles in the desired state so the ideal sintering temperature must be chosen. The selected temperature range, 600–800 °C, should be the proper one to allow the disposal of byproducts and to avoid too high crystallization in phosphate-based powders. The obtained binary glasses were fully amorphous and the crystallinity of the ternary systems was not high thus, it should not disrupt the bioactivity.

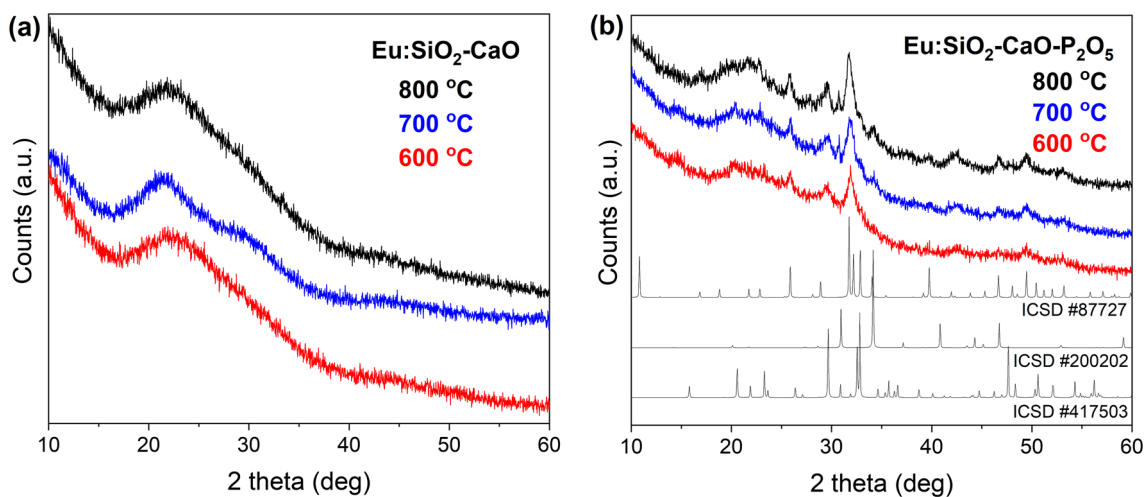
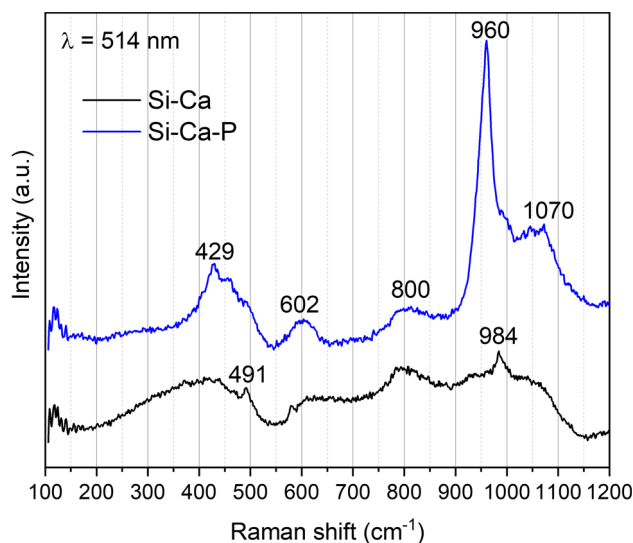


**Fig. 2** X-ray diffraction patterns of  $\text{Eu}^{3+}$ -doped  $\text{SiO}_2\text{-CaO}$  and  $\text{SiO}_2\text{-CaO-P}_2\text{O}_5$  powders annealed at 600 °C, 700 °C, or 800 °C

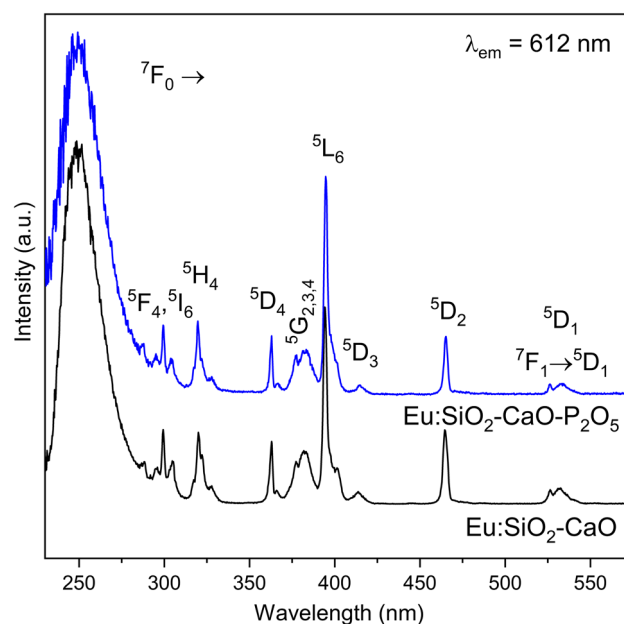
**Fig. 3** Raman spectra of  $\text{Eu}^{3+}$ -doped  $\text{SiO}_2\text{-CaO}$  and  $\text{SiO}_2\text{-CaO-P}_2\text{O}_5$  samples obtained at 700 °C



The Fig. 3 shows the Raman spectra in the 100–1200  $\text{cm}^{-1}$  spectral range of the two samples doped with  $\text{Eu}^{3+}$  ions:  $\text{SiO}_2\text{-CaO}$  and  $\text{SiO}_2\text{-CaO-P}_2\text{O}_5$  annealed at 700 °C. Both spectra exhibit similar spectral features and present the typical bands of silica-based sol-gel glass centered at about 450, 800, and 980  $\text{cm}^{-1}$ . The broadest band observed at around 450  $\text{cm}^{-1}$  is attributed to a network Si–O–Si bending vibration involving adjacent tetrahedral [38]. Sample  $\text{SiO}_2\text{-CaO}$  shows a weak but clear band denoted D1 at 491  $\text{cm}^{-1}$  which is assigned to symmetric stretching modes of Si–O bonds in 4-membered silica rings [38]. The band at 800  $\text{cm}^{-1}$  observed on both spectra is attributed to a Si–O–Si stretching vibrations in silica tetrahedral with a four number of non-bridging oxygens (NBO), in particular to  $\text{SiO}_4^{4-}$  monomers (4 NBO) [39, 40]. The third band visible on the spectrum of  $\text{SiO}_2\text{-CaO}$  at about 980  $\text{cm}^{-1}$  corresponds to Si–OH stretching vibrations of residual silanol groups [38–40]. The Raman spectrum for the sample  $\text{SiO}_2\text{-CaO-P}_2\text{O}_5$  looks slightly different. Visible is the band at 602  $\text{cm}^{-1}$ . At this position appears the D2 band assigned to symmetric stretching modes of O–Si–O, which indicates the presence in the material of cyclic three-membered SiO rings [38].

The differences in the Raman spectra between the two described samples are caused by the addition of  $\text{PO}_4^{3-}$ . The development of the  $\text{SiO}_2\text{-CaO-P}_2\text{O}_5$  network can be identified in the spectrum by the band at approximately 450  $\text{cm}^{-1}$  and the most intense peak at 960  $\text{cm}^{-1}$ . The intensity increase and splitting of the band at lower wavenumbers into two peaks at 430 and 450  $\text{cm}^{-1}$  can be caused by the share of O–P–O bending vibrations of orthophosphate  $\text{PO}_4^{3-}$  units [38, 41, 42]. Additionally, the vibrations of  $\text{PO}_4^{3-}$  contribute to an intensity increase of the band at about 600  $\text{cm}^{-1}$  [38, 43]. At higher wavenumbers (950–1000  $\text{cm}^{-1}$ ), the Si–OH stretching vibrations appear, but on the spectrum of the binary glass, they show weak intensity [43]. The band at 980  $\text{cm}^{-1}$  on the  $\text{SiO}_2\text{-CaO}$  spectrum is assigned to this group. A significant change in this region is caused by the P–O<sup>−</sup> stretching vibrations of phosphate groups at 960  $\text{cm}^{-1}$  [39, 40, 42]. The broad band at 1050  $\text{cm}^{-1}$  is characteristic of calcium-doped glass and reflects  $\text{SiO}_4$  units with one non-bridging oxygen [40, 43]. A low-intensity band at this frequency is observed for the binary glass, while for the ternary system, its intensity increases, which might be related to the higher content of  $\text{Ca}^{2+}$ .

**Fig. 4** Excitation spectra of  $\text{Eu}^{3+}$ -doped  $\text{SiO}_2$ -CaO and  $\text{SiO}_2$ -CaO- $\text{P}_2\text{O}_5$  powders annealed at  $700^\circ\text{C}$



The silicon environment in such glass structures consists of silicon dioxide and glass modifiers. In the case of calcium phosphosilicate glasses,  $\text{SiO}_2$  and  $\text{P}_2\text{O}_5$  are usually network formers and  $\text{CaO}$  is used as a network modifier releasing  $\text{Ca}^{2+}$  ions, which migrate outside the glass. The introduction of  $\text{Ca}^{2+}$  and  $\text{PO}_4^{3-}$  ions changes the silicate network structure by reducing the degree of connectivity in the network by replacing bridging oxygen with non-bridging oxygen [44]. This process leads to the disconnectivity of the glass network and results in the formation of more silanol groups  $\text{Si-OH}$ . Silanol group vibrations are present in the Raman spectra as a small but sharp peak at  $980\text{ cm}^{-1}$  (binary glass) and as the band screened by the sharp intensive peak at  $960\text{ cm}^{-1}$  (ternary glass).

It was considered that some of the phosphates form  $\text{Si-O-P}$  links, and the others might be found as free orthophosphate. It was also reported that for low  $\text{P}_2\text{O}_5$  content, phosphorous is not considered a glass former like silicon, and it is present in the glass structure as  $\text{PO}_4^{3-}$  ions like a glass modifier [44]. The crystallization of phosphates, as observed in the XRD diffractograms of the studied samples, may be caused due to the existence of phosphorous in bioglasses only as a separate orthophosphate phase [12, 45]. If no  $\text{Si-O-P}$  bridges are detected in glasses consisting of  $\text{SiO}_2$ ,  $\text{CaO}$ , and  $\text{P}_2\text{O}_5$ , phosphates are not a part of the silicate glass network, but they rather form isolated orthophosphate units, which take calcium or other cations from the glass network and might be readily released from this material.

### 3.4 Photoluminescence

The photoluminescence excitation spectra for all the samples were registered by monitoring the most intense emission band with a maximum at 612 nm (as will be presented in the next paragraph). There were no significant differences in the spectra among the powders annealed at various temperatures. Two selected spectra of binary and ternary systems annealed at  $700^\circ\text{C}$  are presented in Fig. 4. Among them, no variations in the bands' shapes or positions were observed. The characteristic most intense band with a maximum at 395 nm indicated the excitation from the  ${}^7\text{F}_0$  ground state to the  ${}^5\text{L}_6$  level, and this wavelength was used to register photoluminescence. Other bands in the UV, blue, and green light range corresponded to the excitation to the  ${}^5\text{F}_4$ ,  ${}^5\text{I}_6$ ,  ${}^5\text{H}_4$ ,  ${}^5\text{D}_4$ ,  ${}^5\text{G}_{2,3,4}$ ,  ${}^5\text{D}_3$ ,  ${}^5\text{D}_2$ , and  ${}^5\text{D}_1$  levels. Broad band around 250 nm originated from the charge transfer between europium and oxygen ions in the host.

The emission spectra (Fig. 5) obtained by excitation at 395 nm ( ${}^5\text{L}_6$  level) consisted of typical five bands corresponding to the  ${}^5\text{D}_0 \rightarrow {}^7\text{F}_J$  ( $J = 0, 1, 2, 3,$  and  $4$ ) transitions of  $\text{Eu}^{3+}$  ions. The emission line assigned to the  ${}^5\text{D}_0 \rightarrow {}^7\text{F}_2$  ( $\sim 612\text{ nm}$ ) electric dipole transition is strongly influenced by the electrostatic local field of the luminescent site [22, 46]. Similar dependence is observed for another electric dipole transition  ${}^5\text{D}_0 \rightarrow {}^7\text{F}_0$  ( $\sim 578\text{ nm}$ ) [46]. Transition  ${}^5\text{D}_0 \rightarrow {}^7\text{F}_2$  dominates the emission spectrum when the europium ion is situated in a low symmetry site and occupies a site without an inversion center [22, 47], which is typical for amorphous structures. The third characteristic feature of the  $\text{Eu}^{3+}$  ion is the  ${}^5\text{D}_0 \rightarrow {}^7\text{F}_1$  transition corresponding to the line at about 590 nm [29]. This transition is purely magnetic-dipole, and it is not restricted by any symmetry thus, its intensity is not affected by the environment around  $\text{Eu}^{3+}$  [22, 46]. Eventually, the red-to-orange photoluminescence intensity ratio ( $\text{R/O} = {}^5\text{D}_0 \rightarrow {}^7\text{F}_2/{}^5\text{D}_0 \rightarrow {}^7\text{F}_1$ ) can be an indicator of structural symmetry: the higher the R/O value occurs, the lower local symmetry around  $\text{Eu}^{3+}$  ions exists [20]. Generally, the analysis of the  ${}^5\text{D}_0 \rightarrow {}^7\text{F}_{0,1,2}$  band shapes provides relevant information on the local structure around the RE ion.

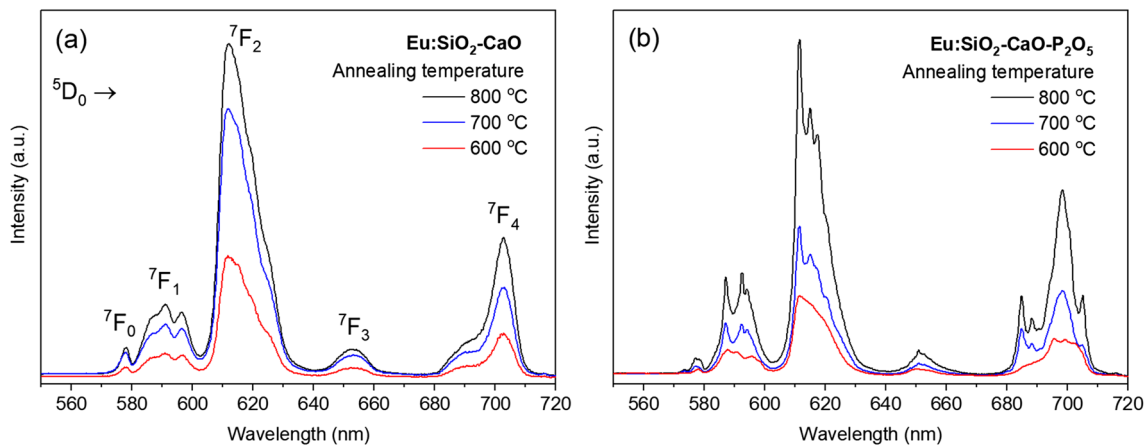


**Fig. 5** Emission of  $\text{Eu}^{3+}$ -doped  $\text{SiO}_2\text{-CaO}$  (a) and  $\text{SiO}_2\text{-CaO-P}_2\text{O}_5$  (b) powders annealed at 600 °C, 700 °C, or 800 °C (under 395 nm excitation)

As can be seen in Fig. 5, the intensity of the emission bands increased with the annealing temperature of the samples. As was expected, the spectra of all samples showed a significantly larger intensity of the  ${}^5\text{D}_0 \rightarrow {}^7\text{F}_2$  emission compared to the  ${}^5\text{D}_0 \rightarrow {}^7\text{F}_1$  transition. The R/O ratio was calculated to be approximately 4.5 for binary glasses. The same ratio for the ternary (and more crystalline) system decreased to around 3. The changed R/O value indicated various  $\text{Eu}^{3+}$  sites with lower symmetry in an amorphous matrix as in the case of  $\text{SiO}_2\text{-CaO}$ . This parameter in the silica-calcia glass was found to be lower than the value reported for silica glass doped with europium (e.g., 6.3 as reported in [20] or 10.9 in [48]), but higher than in other bioactive glasses. In the case of  $\text{Eu}^{3+}$ -doped 45S5 Bioglass, the R/O parameter varied from 3.3 to 2.3, depending on the annealing temperature, as reported in [49]. Similarly, in the case of phosphate glass, the same parameter varied from 3.7 to 2.9, depending on the CaO content, as reported in [23]. For comparison, in crystalline structures, where ions are located in less distorted sites, a higher intensity of  ${}^5\text{D}_0 \rightarrow {}^7\text{F}_1$  emission is observed. Therefore, the R/O parameter for  $\text{Eu}^{3+}$  in different non-amorphous matrices varied as follows: 2.5–2.8 in silica-calcium apatite composites [50], ~2 in hydroxyapatites [51, 52], 1.7 in  $\text{Na}_2\text{Ca}_2\text{Si}_3\text{O}_9$  [53] and < 1 in fluorides nanocrystals in silica glass [54].

A band associated with the  ${}^5\text{D}_0 \rightarrow {}^7\text{F}_0$  transition is another emission peak that can be used to determine the environment of  $\text{Eu}^{3+}$  ions in the lattice. In the binary system samples, one peak was observed with a *lineshape* similar to the spectrum recorded for the  $\text{Eu}^{3+}$ -doped silica xerogel [55]. In the ternary system samples, the splitting of this band was clearly visible, particularly in powders obtained at higher temperatures. This result may indicate that more than one type of  $\text{Eu}^{3+}$  site exists within the  $\text{SiO}_2\text{-CaO-P}_2\text{O}_5$  system [56]. It is well understood because of the presence of both amorphous and crystalline phases in the glass-ceramic structure. The more ordered ions environment in nanocrystals is also observed as better resolved Stark splitting of the bands (Fig. 5b).

The decay curves of the luminescence from the  ${}^5\text{D}_0$  level were recorded at the wavelength corresponding to the maximum intensity of the  ${}^5\text{D}_0 \rightarrow {}^7\text{F}_2$  emission band. Figure 6 displays the decay curves for all the samples and their respective luminescence decay times. The decay rates exhibit a single exponential nature for binary glasses and a slight deviation from this tendency for ternary glass-ceramics. The luminescence lifetimes for  $\text{SiO}_2\text{-CaO}$  samples annealed at different temperatures were equal to 2.40 ms, 3.10 ms, and 3.64 ms for 600 °C, 700 °C, and 800 °C, respectively. This finding is consistent with the observation that higher heat treatment temperature leads to longer decay times due to, among others, a reduction in the number of hydroxide groups [35]. The same tendency was observed for  $\text{SiO}_2\text{-CaO-P}_2\text{O}_5$  but these samples annealed at the same temperature showed shorter luminescence lifetimes (below 3 ms looking at the long-life component of the double-exponential fit as shown in Fig. 6b). When fitted with a single-exponential decay, the lifetimes varied from 1.30 and 2.17 to 2.36 ms increasing successively with the annealing temperature.

The tendency of the longer photoluminescence decay times with the temperature of heat treatment is commonly observed and explained by the reduced OH group content [57]. Hydroxyl quenching is caused by residual water, solvents, and silanol groups present in the sol-gel glasses, which leads to an enhancement of nonradiative decay pathways of RE ions by dipole-dipole interactions. The OH concentration is reduced or eliminated by the heat treatment. As a consequence, the luminescence lifetimes increase with the temperature of thermal treatment, as was observed in the investigated samples. Furthermore, it is claimed that the crystallization of glass components reduces the lifetime of the  ${}^5\text{D}_0$  emitting level because it resists ion mobility and their exchange, which gives rise to a higher transition probability [23]. This is the probable cause behind the shorter luminescence lifetimes observed in samples of the ternary system as compared to those of the binary system. As discussed earlier, all the phosphate-based glasses showed partial crystallization, while all the samples of silica-calcia glass were amorphous (Fig. 2). As previously reported, the calcium content in the phosphate glass (10 mol% < CaO < 30 mol%) and silica-based glass (CaO > 23 mol%) was also indicated as a factor that affects luminescence lifetime. An increase in the concentration of  $\text{Ca}^{2+}$  caused a reduction in luminescence lifetime, as explained by the location of  $\text{Eu}^{3+}$  ions in different sites [23, 30].

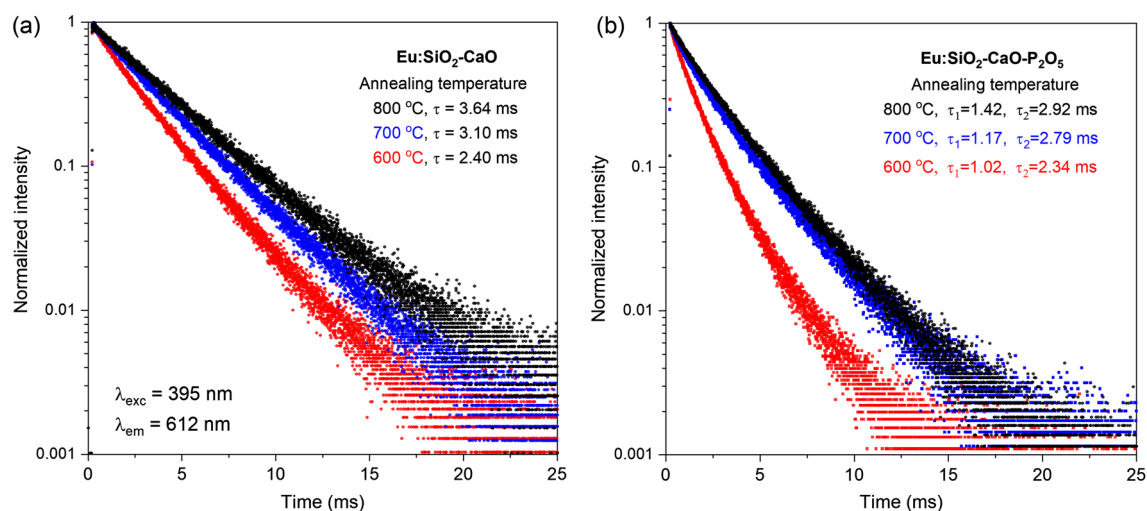


**Fig. 6** Decay dynamics of  $\text{Eu}^{3+}\text{D}_0$  level in  $\text{SiO}_2\text{--CaO}$  (a) and  $\text{SiO}_2\text{--CaO--P}_2\text{O}_5$  (b) powders annealed at 600 °C, 700 °C, or 800 °C

## 4 Conclusions

Glass particles of the  $\text{Eu}^{3+}$ -doped  $\text{SiO}_2\text{--CaO}$  binary and  $\text{SiO}_2\text{--CaO--P}_2\text{O}_5$  ternary systems were prepared by the sol–gel method. The introduction of  $\text{PO}_4^{3-}$  groups using phosphoric acid did not significantly affect the morphology of the samples. All particles were not aggregated with a spherical shape having an average size of approximately 100 nm (103 vs. 107 nm for  $\text{SiO}_2\text{--CaO}$  and  $\text{SiO}_2\text{--CaO--P}_2\text{O}_5$ , respectively). The annealing temperature (600–800 °C) did not modify the morphology and structure of the samples either. In the structure of the phosphate-based systems, crystalline phases were evident, while the binary glass was fully amorphous. The photoluminescent properties of the powders were influenced by the presence of crystallites, resulting in variation of the spectrum profile and shorter luminescence lifetimes for the ternary glass–ceramics. The higher temperature during heat treatment led to higher emission intensity, more visible Stark splitting, and longer luminescence lifetimes, mainly due to the removal of silanol groups and a higher degree of crystallinity. These results confirm that europium spectroscopy enables a nondestructive, diagnostic means of probing the crystallization in the bioactive glass samples.

**Acknowledgements** The authors would like to acknowledge I. Jakobowska, E. Bukowska, D. Szymanski, and A. Baszczuk for their help in experiments and measurements.

**Funding** This work was supported by the National Science Centre (G. No. 2016/22/E/ST5/00530).

**Data Availability Statement** This manuscript has associated data in a data repository. [Authors' comment: The authors declare that the data supporting the findings of this study are available within the paper. Should any raw data files be needed they are available from the corresponding authors upon reasonable request.]

## Declarations

**Conflicts of interests** The authors have no relevant financial or non-financial interests to disclose.

## References

- M.H. Kaou, M. Furkó, K. Balázs, C. Balázs, *Nanomaterials* **13**, 2287 (2023)
- A. Hoppe, N.S. Güldal, A.R. Boccaccini, *Biomaterials* **32**, 2757–2774 (2011). <https://doi.org/10.1016/j.biomaterials.2011.01.004>
- M. Dong, G. Jiao, H. Liu, W. Wu, S. Li, Q. Wang, D. Xu, X. Li, Y. Huan Liu, *Biol. Trace Elem. Res.* **173**, 306–315 (2016). <https://doi.org/10.1007/s12011-016-0686-3>
- H. Zhou, G. Jiao, M. Dong, H. Chi, H. Wang, W. Wu, H. Liu, S. Ren, M. Kong, C. Li, L. Zhang, Y. Chen, *Biol. Trace Elem. Res.* **190**, 327–335 (2019). <https://doi.org/10.1007/s12011-018-1574-9>
- P. Saravanapavan, J.R. Jones, R.S. Pryce, L.L. Hench, *J. Biomed. Mater. Res.* **66A**, 110 (2003). <https://doi.org/10.1002/jbm.a.10532>
- X. Wang, X. Li, A. Ito, Y. Sogo, *Acta Biomater.* **7**, 3638–3644 (2011). <https://doi.org/10.1016/j.actbio.2011.06.029>
- L.-C. Gerhardt, A.R. Boccaccini, *Materials* **3**, 3867–3910 (2010). <https://doi.org/10.3390/ma3073867>



8. S. Labbaf, O. Tsigkou, K.H. Müller, M.M. Stevens, A.E. Porter, J.R. Jones, *Biomaterials* **32**, 1010–1018 (2011). <https://doi.org/10.1016/j.biomaterials.2010.08.082>
9. M. Vallet-Regí, C.V. Ragel, A.J. Salinas, Glasses with medical applications. *Eur. J. Inorg. Chem.* **2003**, 1029–1042 (2003). <https://doi.org/10.1002/ejic.200390134>
10. A. Martínez, I. Izquierdo-Barba, M. Vallet-Regí, *Chem. Mater.* **12**, 3080–3088 (2000). <https://doi.org/10.1021/cm001107o>
11. J.R. Jones, O. Tsigkou, E.E. Coates, M.M. Stevens, J.M. Polak, L.L. Hench, *Biomaterials* **28**, 1653–1663 (2007). <https://doi.org/10.1016/j.biomaterials.2006.11.022>
12. R.G. Hill, D.S. Brauer, *J. Non-Cryst. Solids* **357**, 3884–3887 (2011). <https://doi.org/10.1016/j.jnoncrysol.2011.07.025>
13. A.J. Salinas, S. Shruti, G. Malavasi, L. Menabue, M. Vallet-Regí, *Acta Biomater.* **7**, 3452–3458 (2011). <https://doi.org/10.1016/j.actbio.2011.05.033>
14. A. Hoppe, A. Brandl, O. Bleiziffer, A. Arkudas, R.E. Horch, B. Jokic, D. Janackovic, A.R. Boccaccini, *Mater. Sci. Eng. C* **57**, 157–163 (2015). <https://doi.org/10.1016/j.msec.2015.07.014>
15. J. Lao, E. Jallot, J.-M. Nedelec, *J. Mater. Chem.* **19**, 2940–2949 (2009). <https://doi.org/10.1039/b822214b>
16. M. Bellantone, H.D. Williams, L.L. Hench, *Antimicrob. Agents Chemother.* **46**, 1940–1945 (2002). <https://doi.org/10.1128/AAC.46.6.1940-1945.2002>
17. A.C.M. Renno, P.S. Bossini, M.C. Crovace, A.C.M. Rodrigues, E.D. Zanotto, N.A. Parizotto, *BioMed. Res. Int.* **2013**, 141427 (2013). <https://doi.org/10.1155/2013/141427>
18. M. Brink, T. Turunen, R.P. Haponnen, A. Yli-Urpo, *J. Biomed. Mater. Res.* **37**, 114–121 (1997)
19. J.R. Jones, *J. Eur. Ceram. Soc.* **29**, 1275–1281 (2009). <https://doi.org/10.1016/j.jeurceramsoc.2008.08.003>
20. R. Reisfeld, E. Zigansky, M. Gaft, *Mol. Phys.* **102**, 1319–1330 (2004). <https://doi.org/10.1080/00268970410001728609>
21. V.C. Costa, M.J. Lochhead, K.L. Bray, *Chem. Mater.* **8**, 783–790 (1996). <https://doi.org/10.1021/cm9504910>
22. E.J. Nassar, K.J. Ciuffi, L.C. Calefi, L.L. Avila, L.C. Bandeira, A. Cestari, E.H. de Faria, A.L. Marçal, M.G. Matos, *Europium III: Different emission spectra in different matrices, the same element*, In: *Europium: Compounds, Production and Applications*, ed. by L.M. Moreno, (Nova Science Publishers Inc., New York, 2009)
23. Ch.S. Rao, K.U. Kumar, C.K. Jayasankar, *Solid State Sci.* **13**, 1309–1314 (2011). <https://doi.org/10.1016/j.solidstatesciences.2011.03.027>
24. G. Li, G. Liang, S. Zhao, K. Ma, W. Feng, D. Zhou, X. Liu, *Adv. Appl. Ceram.* **114**, 164–174 (2015). <https://doi.org/10.1179/1743676114Y.0000000210>
25. Y. Fan, P. Yang, S. Huang, J. Jiang, H. Lian, J. Lin, *J. Phys. Chem. C* **113**, 7826–7830 (2009). <https://doi.org/10.1021/jp900515x>
26. C. Wu, L. Xia, P. Han, L. Mao, J. Wang, D. Zhai, B. Fang, J. Chang, Y. Xiao, *A.C.S. Appl. Mater. Interfaces* **8**, 11342–11354 (2016). <https://doi.org/10.1021/acsami.6b03100>
27. S. Huang, X. Kang, Z. Cheng, P. Ma, Y. Jia, J. Lin, *J. Colloid Interface Sci.* **387**, 285–291 (2012). <https://doi.org/10.1016/j.jcis.2012.08.004>
28. A. Baranowska, M. Kochanowicz, J. Żmojda, P. Miluski, M. Leśniak, D. Dorosz, *Proc SPIE* **11045**, Opt. Fibers Appl. **2018**, 1104505 (2019). <https://doi.org/10.1117/12.2522250>
29. Y. Xue, Y. Du, J. Yan, Z. Liu, P.X. Ma, X. Chen, B. Lei, *J. Mater. Chem. B* **3**, 3831–3839 (2015). <https://doi.org/10.1039/C5TB00204D>
30. J.K. Krebs, J.M. Brownstein, J.T. Gibides, *J. Lumin.* **128**, 780–782 (2008). <https://doi.org/10.1016/j.jlumin.2007.12.008>
31. A.M. Deliormanli, S. Oguzlar, M. Zeyrek Ongun, *J. Mater. Res.* **37**, 622–635 (2022). <https://doi.org/10.1557/s43578-021-00461-6>
32. A.M. Deliormanli, B. Rahman, S. Oguzlar, M. Zeyrek Ongun, *J. Alloys. Compd.* **944**, 169153 (2023). <https://doi.org/10.1016/j.jallcom.2023.169153>
33. A.M.B. Silva, L.S. Jesus, W. Correa, D.O. Junot, L.V.E. Caldas, N.O. Dantas, D.N. Souza, A.C.A. Silva, *Appl. Radiat. Isot.* **201**, 110997 (2023). <https://doi.org/10.1016/j.apradiso.2023.110997>
34. A. Lukowiak, J. Lao, J. Lacroix, J.-M. Nedelec, *Chem. Commun.* **49**, 6620–6622 (2013). <https://doi.org/10.1039/c3cc00003f>
35. B. Borak, J. Krzak, M. Ptak, W. Strek, A. Lukowiak, *J. Mol. Struct.* **1166**, 48–53 (2018). <https://doi.org/10.1016/j.molstruc.2018.04.019>
36. S. Murakami, M. Herren, D. Rau, M. Morita, *Inorg. Chim. Acta* **300–302**, 1014–1021 (2000). [https://doi.org/10.1016/S0020-1693\(00\)00008-6](https://doi.org/10.1016/S0020-1693(00)00008-6)
37. Z. Hong, R.L. Reis, J.F. Mano, *J. Biomed. Mater. Res. A* **88**, 304–313 (2009). <https://doi.org/10.1002/jbm.a.31848>
38. O. Cristini-Robbe, K. Raulin, F. Dubart, R. Bernard, C. Kinowski, N. Damene, I. El Yazidi, A. Boed, S. Turrell, *J. Mol. Struct.* **1050**, 232–237 (2013). <https://doi.org/10.1016/j.molstruc.2013.06.063>
39. M. Wang, J. Cheng, M. Li, F. He, *Phys. B* **406**, 3865–3869 (2011). <https://doi.org/10.1016/j.physb.2011.07.014>
40. D. Bellucci, G. Bolelli, V. Cannillo, A. Cattini, A. Sola, *Mater. Charact.* **62**, 1021–1028 (2011). <https://doi.org/10.1016/j.matchar.2011.07.008>
41. A. Antonakos, E. Liarokapis, T. Leventouri, *Biomaterials* **28**, 3043–3054 (2007). <https://doi.org/10.1016/j.biomaterials.2007.02.028>
42. F. Errassifi, S. Sarda, A. Barroug, A. Legrouri, H. Sfihi, C. Rey, *J. Colloid Interface Sci.* **420**, 101–111 (2014). <https://doi.org/10.1016/j.jcis.2014.01.017>
43. A.K. Yadav, P. Singh, *RSC Adv.* **5**, 67583–67609 (2015). <https://doi.org/10.1039/c5ra13043c>
44. A. Lucas-Girot, F.Z. Mezahi, M. Mami, H. Oudadesse, A. Harabi, M.L. Floch, *J. Non-Cryst. Solids* **357**, 3322–3327 (2011). <https://doi.org/10.1016/j.jnoncrysol.2011.06.002>
45. A. Pedone, T. Charpentier, G. Malavasi, M.C. Menziani, *Chem. Mater.* **22**, 5644–5652 (2010). <https://doi.org/10.1021/cm102089c>
46. H. Fneich, N. Gaumer, S. Chaussedent, W. Blanc, A. Mehdi, *Molecules* **23**, 1768 (2018). <https://doi.org/10.3390/molecules23071768>
47. K. Binnemans, Interpretation of europium(III) spectra. *Coord. Chem. Rev.* **295**, 1–45 (2015). <https://doi.org/10.1016/j.ccr.2015.02.015>
48. S. Han, Y. Du, J. Yuan, Y. Tao, Y. Wang, S. Yan, D. Chen, *J. Non-Cryst. Solids* **532**, 119894 (2020). <https://doi.org/10.1016/j.jnoncrysol.2020.119894>
49. A. Baranowska, M. Leśniak, M. Kochanowicz, J. Żmojda, P. Miluski, D. Dorosz, *Materials* **13**, 1281 (2020). <https://doi.org/10.3390/ma13061281>
50. A. Isobe, S. Takeshita, T. Isobe, *Langmuir* **31**, 1811–1819 (2015). <https://doi.org/10.1021/la503652w>
51. T.A.R.M. Lima, M.E.G. Valerio, *J. Lumin.* **201**, 70–76 (2018). <https://doi.org/10.1016/j.jlumin.2018.04.043>
52. M. Long, F. Hong, W. Li, F. Li, H. Zhao, Y. Lv, H. Li, F. Hu, L. Sun, C. Yan, Z. Wei, *J. Lumin.* **128**, 428–436 (2008). <https://doi.org/10.1016/j.jlumin.2007.09.012>
53. Y. Zhu, C. Tong, R. Dai, C. Xu, L. Yang, Y. Li, *Mater. Lett.* **213**, 245–248 (2018). <https://doi.org/10.1016/j.matlet.2017.11.082>
54. P. Luo, P. Huang, J. Wang, C. Yao, Y. Zhao, B. Zhou, Q. Zheng, X. Zhang, W. Jiang, L. Wang, *J. Am. Ceram. Soc.* **103**, 3089–3096 (2020). <https://doi.org/10.1111/jace.17021>
55. R. Camprostrini, G. Carturan, M. Ferrari, M. Montagna, O. Pilla, *J. Mater. Res.* **7**, 745–753 (1992). <https://doi.org/10.1557/JMR.1992.0745>
56. A. Doat, F. Pelle, N. Gardant, A. Lebugle, *J. Solid State Chem.* **177**, 1179–1187 (2004). <https://doi.org/10.1016/j.jssc.2003.10.023>
57. A. Monteil, S. Chaussedent, G. Alombert-Goget, N. Gaumer, J. Obriot, S.J.L. Ribeiro, Y. Messaddeq, A. Chiasera, M. Ferrari, *J. Non-Cryst. Solids* **348**, 44 (2004). <https://doi.org/10.1016/j.jnoncrysol.2004.08.124>